Assessment of the Sonic-Eddy Model in Hypersonic Turbulent Boundary Layers

Priyanshu Singh

A thesis

submitted in partial fulfillment of the

requirements for the degree of

Master of Science in Aeronautics and Astronautics

University of Washington

2026

Committee:

Robert Breidenthal

Carl Knowlen

Program Authorized to Offer Degree:

Department of Aeronautics and Astronautics

University of Washington

Abstract

Assessment of the Sonic-Eddy Model in Hypersonic Turbulent Boundary Layers

Priyanshu Singh

Chair of the Supervisory Committee:

Robert Breidenthal

Department of Aeronautics and Astronautics

Hypersonic turbulent boundary layers exhibit strong compressibility and acoustic effects that alter turbulent momentum transport and complicate the interpretation of near-wall structure. A central unresolved question is how finite acoustic signaling speed limits the size, coherence, and effectiveness of the eddies responsible for transferring momentum across the boundary layer. This thesis evaluates the sonic-eddy transport model, in which turbulent transport is constrained by eddies for which the acoustic communication time across the eddy is comparable to or shorter than the eddy turnover time. Under this framework, the outer region of the boundary layer acts as a bottleneck for momentum transfer from the freestream to the wall, leading to specific predictions for eddy-size variation and skin-friction scaling with Mach number. Three-dimensional viscous-sublayer-resolved Reynolds-stress-model computations of hypersonic turbulent boundary layers were used to examine these predictions and to assess the extent to which the sonic-eddy model is consistent with the computed mean flow behavior. The results are broadly consistent with the key predictions of the sonic-eddy transport model and provide insight into its validity and limitations for hypersonic wall-bounded turbulence.

TABLE OF CONTENTS

LIST OF FIGURES

NOMENCLATURE

a	Local speed of sound
a_∞	Freestream speed of sound
a_t	Stagnation speed of sound
C_f	Skin-friction coefficient
M_∞	Freestream Mach number
Re'	Unit Reynolds number
Re_x	Freestream Reynolds number based on x
u_τ	Friction velocity
U_∞	Freestream velocity
x	Streamwise coordinate
y	Wall-normal coordinate
z	Spanwise coordinate
y^+	Wall-normal coordinate in wall units
y_d	Diffusion-limit wall-normal location
δ	Boundary-layer thickness
$\lambda*$	Sonic-eddy size
λ	Eddy length scale
ρ_∞	Freestream density
ρ_w	Density at wall
μ_∞	Freestream dynamic viscosity
μ_w	Wall dynamic viscosity
ν_w	Wall kinematic viscosity
τ_w	Wall shear stress
γ	Ratio of specific heats
R_{ij}	Favre-averaged Reynolds-stress component
t_a	Acoustic communication time
t_e	Eddy turnover time
δ_{99}	Boundary-layer thickness
ε_t	Effective eddy diffusivity

CHAPTER 1: Introduction

1.1 Background and Motivation

Hypersonic turbulent boundary layers arise in a wide range of high-speed aerodynamic applications, including atmospheric re-entry vehicles, high-speed air-breathing propulsion systems, and external surfaces exposed to extreme aerodynamic loading. In these flows, the interaction between turbulence, compressibility, and thermodynamic variation governs the transport of momentum and energy between the freestream and the wall. As a result, the behavior of the boundary layer plays a central role in determining aerodynamic drag, surface heating, and the overall performance and survivability of hypersonic systems [10].

The structure of a turbulent boundary layer is especially important because wall-bounded turbulence directly controls quantities of primary engineering interest, including wall shear stress, skin-friction drag, and heat transfer. These quantities influence vehicle efficiency, thermal protection system requirements, and the design of inlets and internal flow passages. Accurate physical interpretation of momentum transport within the boundary layer is therefore essential not only for predictive modeling, but also for the development of reduced-order scaling arguments and turbulence closures appropriate for hypersonic conditions.

In incompressible wall turbulence, near-wall structure is commonly interpreted through inner scaling arguments based on viscous length and velocity scales. In hypersonic turbulent boundary layers, however, this interpretation becomes more complicated because the flow is strongly affected by compressibility, variable density, and temperature-dependent viscosity. These effects alter both the local state of the fluid and the manner in which turbulent eddies exchange momentum across the boundary layer. Consequently, classical intuition developed for incompressible turbulence does not always provide a complete physical description of transport in the hypersonic regime.

This motivates the need for a framework that interprets turbulent transport not only through nondimensional scaling, but also through the physical mechanisms that limit the size and effectiveness of the eddies responsible for momentum transfer. Of particular interest is the possibility that finite acoustic signaling speed constrains coherent turbulent motion, thereby modifying how momentum is transmitted from the freestream toward the wall near the edge of the boundary layer. Understanding this transport process is central to interpreting skin-friction behavior and to assessing physics-based models for hypersonic wall-bounded turbulence.

1.2 Classical Perspectives on Near-Wall Scaling and Momentum Transport

In wall-bounded turbulent flows, the near-wall region is commonly interpreted using inner scaling based on quantities defined by the wall shear stress. The friction velocity provides a characteristic velocity scale, while the viscous length scale provides a corresponding length scale for the inner region. These quantities lead naturally to wall units, in which distances and velocities are nondimensionalized to examine the behavior of mean quantities close to the wall. This framework has played a central role in the interpretation of canonical incompressible turbulent boundary layers, channels, and pipe flows.

$$u_\tau = \sqrt{\frac{\tau_w}{\rho_w}}, \quad u^+ = \frac{u}{u_\tau}, \quad y^+ = \frac{\rho_w u_\tau y}{\mu_w} = \frac{y u_\tau}{\nu_w}$$

The usefulness of inner scaling lies in its ability to reveal common structure in the near-wall region across different flow conditions. When expressed in wall units, the mean velocity profile and many turbulence statistics often exhibit approximate similarity, allowing the flow to be interpreted in terms of viscous, buffer, logarithmic, and outer regions. In this sense, classical inner scaling provides both a compact description of near-wall behavior and a practical foundation for reduced-order laws, empirical correlations, and turbulence modeling strategies.

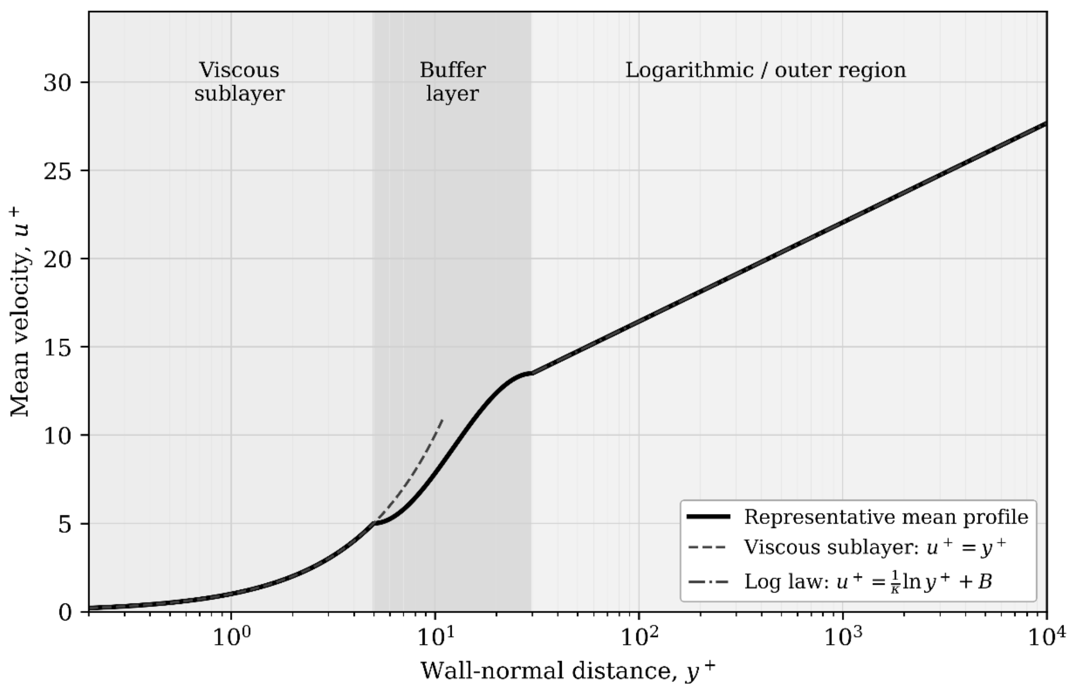

Figure 1.1: Schematic of the classical law-of-the-wall velocity profile, showing the viscous sublayer, buffer layer, and logarithmic/outer region. The reference relations $u^+ = y^+$ and $u^+ = (1/\kappa) \ln y^+ + B$ are shown using $\kappa = 0.41$ and $B = 5.2$.

For compressible and hypersonic turbulent boundary layers, however, the interpretation becomes more complicated because density, temperature, and viscosity can vary strongly across the flow. As a result, direct application of incompressible wall scaling is often insufficient. A number of compressibility-aware transformations have therefore been introduced to extend inner scaling concepts to high-speed flows, including the classical Van Driest transformation and related approaches motivated by Morkovin's hypothesis [6,7]. A representative form of the Van Driest transformation is

$$u_{VD}^{+} = \int_{0}^{u^{+}} \left(\frac{\rho}{\rho_w}\right)^{1/2} du^{+}$$

which accounts for density variation in the mean velocity scaling **[6]**. Related ideas such as Reynolds analogy have also been used to connect momentum and thermal behavior in compressible boundary layers and to interpret the relation between skin friction and heat transfer [8].

Although such approaches are valuable for collapse, comparison, and interpretation, they primarily reorganize the observed flow behavior rather than directly identifying the physical mechanism that limits turbulent momentum transfer in hypersonic conditions. In particular, they do not explicitly address whether compressibility or acoustic signaling imposes a constraint on the size, coherence, or transport effectiveness of the eddies responsible for carrying momentum across the boundary layer. This distinction motivates the need for a more explicitly transport-based framework, which is introduced in the next section through the sonic-eddy model.

1.3 Sonic-Eddy Transport Model

A more explicitly transport-based interpretation of hypersonic turbulent boundary layers is provided by the sonic-eddy model. Originally introduced as a model for compressible turbulence and later specialized to hypersonic boundary-layer flow, the central idea is that the eddies most responsible for momentum transfer cannot remain dynamically coherent unless acoustic communication across the eddy is sufficiently rapid. In this view, the finite speed of acoustic signaling does not merely affect how the flow is scaled; it places a physical constraint on the size of the coherent structures that can effectively transport momentum [1-3].

The model may be interpreted through a competition between two characteristic timescales. For an eddy of size λ embedded in a mean shear dU/dy, the rotational velocity scale is of order $\lambda\,(dU/dy)$, so the eddy turnover time scales as

$$t_e \sim \frac{1}{dU/dy}$$

The acoustic communication time across the eddy scales as

$$t_a \sim \frac{\lambda}{a}$$

where a is the local speed of sound. The largest eddy that can remain coherent is then obtained by requiring the acoustic communication time to be comparable to or shorter than the eddy turnover time. This defines a sonic-eddy size,

$$\lambda^* \sim \frac{a}{dU/dy}$$

which provides a local upper bound on the size of the eddies that can efficiently participate in turbulent transport [1,3].

A key consequence of this model is that the sonic-eddy size varies across the boundary layer because both the local sound speed and the mean shear vary with wall-normal position. Under the simplified hypersonic boundary-layer framework proposed by Breidenthal, this variation implies that the effective transporting eddies are largest in the inner part of the layer and smallest near the outer edge. The outer region therefore becomes the slowest location for momentum to cross the boundary layer, so it acts as a bottleneck for momentum transfer from the freestream toward the wall. In this interpretation, the wall shear is controlled not only by near-wall dynamics, but also by the rate at which momentum can be supplied through the outer portion of the layer [2].

This transport-limiting viewpoint leads to concrete predictions that can be examined against simulation data. In particular, the model yields explicit trends for the wall-normal variation of sonic-eddy size and, under additional simplifying assumptions, a skin-friction scaling of the form [2,3]

$$C_f \propto \frac{1}{M_\infty}$$

These predictions are especially relevant to the present work because they connect a physically motivated transport constraint to measurable boundary-layer quantities. The objective of this thesis is therefore not only to examine inner-scaled behavior, but also to assess the extent to which wall-resolved Reynolds-stress-model computations of hypersonic turbulent boundary layers are consistent with the sonic-eddy interpretation of momentum transport.

1.4 Research Gap and Questions

The sonic-eddy transport model provides a physically appealing interpretation of momentum transfer in hypersonic turbulent boundary layers by relating coherent turbulent transport to acoustic communication and local mean shear. In contrast to classical scaling approaches, which primarily aim to collapse or reorganize the observed flow behavior, the sonic-eddy model offers a mechanism-based explanation for how compressibility may constrain the size and effectiveness of the eddies responsible for carrying momentum across the boundary layer. This leads to specific predictions for the wall-normal variation of sonic-eddy size, the role of the outer region as a transport bottleneck, and the resulting dependence of skin friction on Mach number.

Despite this appealing physical interpretation, the extent to which the sonic-eddy model is consistent with numerical simulations of hypersonic turbulent boundary layers remains insufficiently established. In particular, its predictions must be examined against computed flow behavior to determine whether the model captures the dominant transport trends over the range of conditions considered in the present work. This motivates the need for a careful assessment of the sonic-eddy interpretation using viscous-sublayer-resolved Reynolds-stress-model simulations.

The present thesis is guided by several related questions concerning the validity of the sonic-eddy interpretation of momentum transport in hypersonic turbulent boundary layers. In particular, this work examines the extent to which the computed boundary-layer behavior remains consistent with the sonic-eddy framework and whether the outer portion of the layer behaves as a bottleneck for momentum transfer from the freestream toward the wall, as proposed by the model. It also considers whether the predicted wall-normal variation of sonic-eddy size is reflected in the simulation results and whether the computed skin-friction trends exhibit behavior consistent with the Mach-number dependence implied by the sonic-eddy theory. More broadly, the present study seeks to identify the principal strengths, limitations, and apparent range of validity of the sonic-eddy transport model for the cases considered.

These questions define the central scope of the present work. The objective is not only to assess whether the model provides a useful qualitative interpretation of hypersonic wall-bounded turbulence, but also to examine how well its main transport-based predictions are supported by the computed mean flow behavior.

1.5 Objectives and Contributions

The objective of the present thesis is to evaluate the sonic-eddy transport model as a physics-based framework for interpreting momentum transfer in hypersonic turbulent boundary layers using viscous-sublayer-resolved Reynolds-stress-model simulations. Rather than relying only on classical transformed scaling, the present work examines whether a transport-based description rooted in acoustic constraints on coherent eddies provides a useful interpretation of the computed flow behavior.

The main contribution of this thesis is an assessment of the sonic-eddy framework against numerical results for hypersonic wall-bounded turbulence. By comparing the central predictions of the model with simulation data, this study provides a transport-based perspective on hypersonic turbulent boundary layers and clarifies the extent to which the sonic-eddy interpretation is supported in the cases considered. In addition, the thesis identifies the practical strengths and limitations of this framework and shows how it complements more traditional inner-scaling approaches used in compressible turbulence analysis.

1.6 Thesis Organization

The remainder of this thesis is organized as follows. Chapter 2 presents the theoretical framework underlying the sonic-eddy transport model and describes the numerical methodology used in the present study. Chapter 3 presents the simulation results and discusses them in the context of the sonic-eddy interpretation, with particular attention to eddy-size variation, momentum-transfer behavior, and skin-friction trends. Finally, Chapter 4 summarizes the main conclusions of the thesis.

CHAPTER 2: Theoretical Framework and Numerical Methodology

2.1 The Sonic-Eddy Model for Hypersonic Boundary Layers

A transport-based interpretation of compressible turbulence is provided by the sonic-eddy model, originally introduced by Breidenthal for compressible turbulent flows and later specialized to the hypersonic turbulent boundary layer. In this framework, the effect of Mach number on turbulence is attributed primarily to the finite speed of acoustic signaling rather than directly to density variation itself. The central idea is that turbulent momentum transfer is controlled by the largest dynamically active eddies that are still able to maintain coherence in a compressible flow.

In Breidenthal's simplified model of the hypersonic boundary layer, three assumptions are introduced to obtain a tractable physical description. First, the mean streamwise velocity profile is assumed to be approximately linear across the boundary layer. Second, the total enthalpy is assumed uniform. Third, turbulent transport is assumed to be controlled by sonic eddies, namely eddies whose rotational Mach number is of order unity. These assumptions convert the hypersonic boundary layer into a model problem in which the transport-limiting role of acoustic signaling can be examined directly.

The physical basis of the model is the requirement that an eddy must communicate across its own diameter during a characteristic rotation in order to behave as a coherent transporting structure. If acoustic signaling across the eddy is too slow relative to the eddy's rotational motion, the eddy can no longer sustain the non-steady coordination needed for efficient turbulent transport. Under this interpretation, the finite acoustic signaling speed associated with compressibility imposes a physical upper limit on the size of the eddies that can actively transfer momentum. The largest eddy satisfying this requirement is referred to as the sonic eddy.

When this idea is applied to a hypersonic boundary layer, it leads naturally to a transport-limited view of wall-bounded turbulence. Because the local sound speed and mean shear vary across the layer, the largest coherent transporting eddies are not expected to be uniform in size. This provides the basis for the wall-normal variation of sonic-eddy size, the interpretation of the outer region as a bottleneck for momentum transfer, and the resulting skin-friction trends developed in the following section. Section 2.2 therefore formalizes these ideas through the derivation of the sonic-eddy scaling relations used throughout the remainder of this thesis.

2.2 Derivation of Sonic-Eddy Scaling Relations

The sonic-eddy model is based on the idea that an eddy can act as an effective transporting structure only if information associated with non-steady motion can propagate across the eddy during one characteristic rotation. In a shear flow, an eddy of size λ experiences a characteristic rotational velocity of order $\lambda\ (dU/dy)$, so its turnover time scales as

$$t_e \sim \frac{\lambda}{\lambda(\,dU/dy)} \sim \left(\frac{dU}{dy}\right)^{-1}$$

The corresponding acoustic communication time across the eddy is

$$t_a \sim \frac{\lambda}{a}$$

where a is the local speed of sound. The largest dynamically active eddy is then identified by the condition $t_a \sim t_e$, or equivalently by requiring its rotational Mach number to be of order unity. This defines the sonic-eddy size

$$\lambda^* \sim \frac{a}{dU/dy}$$

Thus, the largest eddy capable of efficient momentum transport is set by the competition between local mean shear and acoustic signaling.

To apply this idea to an idealized hypersonic turbulent boundary layer, Breidenthal assumes that the mean velocity profile is approximately linear and that the total enthalpy is uniform across the layer. The linear-profile assumption is motivated by the Mach 6 measurements of Neeb et al. (2018), who reported that the mean velocity profile in a hypersonic boundary layer is remarkably linear. With this idealized representation,

$$\frac{u}{U_\infty} = \frac{y}{\delta}, \ \frac{dU}{dy} = \frac{U_\infty}{\delta}$$

so that the sonic-eddy size becomes

$$\frac{\lambda^*}{\delta} = \frac{a}{U_\infty}$$

Uniform total enthalpy implies

$$a^2 = a_t^2 - \frac{\gamma - 1}{2} u^2$$

where a_t is the stagnation speed of sound. Using the freestream Mach number $M_\infty = U_\infty / a_\infty$, this may be written as

$$\left(\frac{a_t}{U_\infty}\right)^2 = \frac{\gamma - 1}{2} + \frac{1}{M_\infty^2}$$

Substituting into the sonic-eddy relation gives

$$\frac{\lambda^*}{\delta} = \frac{a}{U_\infty} = \left[\left(\frac{a_t}{U_\infty}\right)^2 - \frac{\gamma - 1}{2}\left(\frac{u}{U_\infty}\right)^2\right]^{1/2}$$

and, with $u/U_\infty = y/\delta$,

$$\frac{\lambda^*}{\delta} = \left[\frac{\gamma - 1}{2} + \frac{1}{M_\infty^2} - \frac{\gamma - 1}{2}\left(\frac{y}{\delta}\right)^2\right]^{1/2}$$

This expression provides the wall-normal variation of the sonic-eddy size in the idealized hypersonic boundary layer.

The wall-normal variation implied by this relation is shown schematically in Figure 2.1. The sonic-eddy size is largest near the wall and decreases toward the outer edge of the boundary layer, where it reaches $1/M_\infty$. This reduction in sonic-eddy size near the boundary-layer edge is central to the interpretation of the outer region as a transport bottleneck.

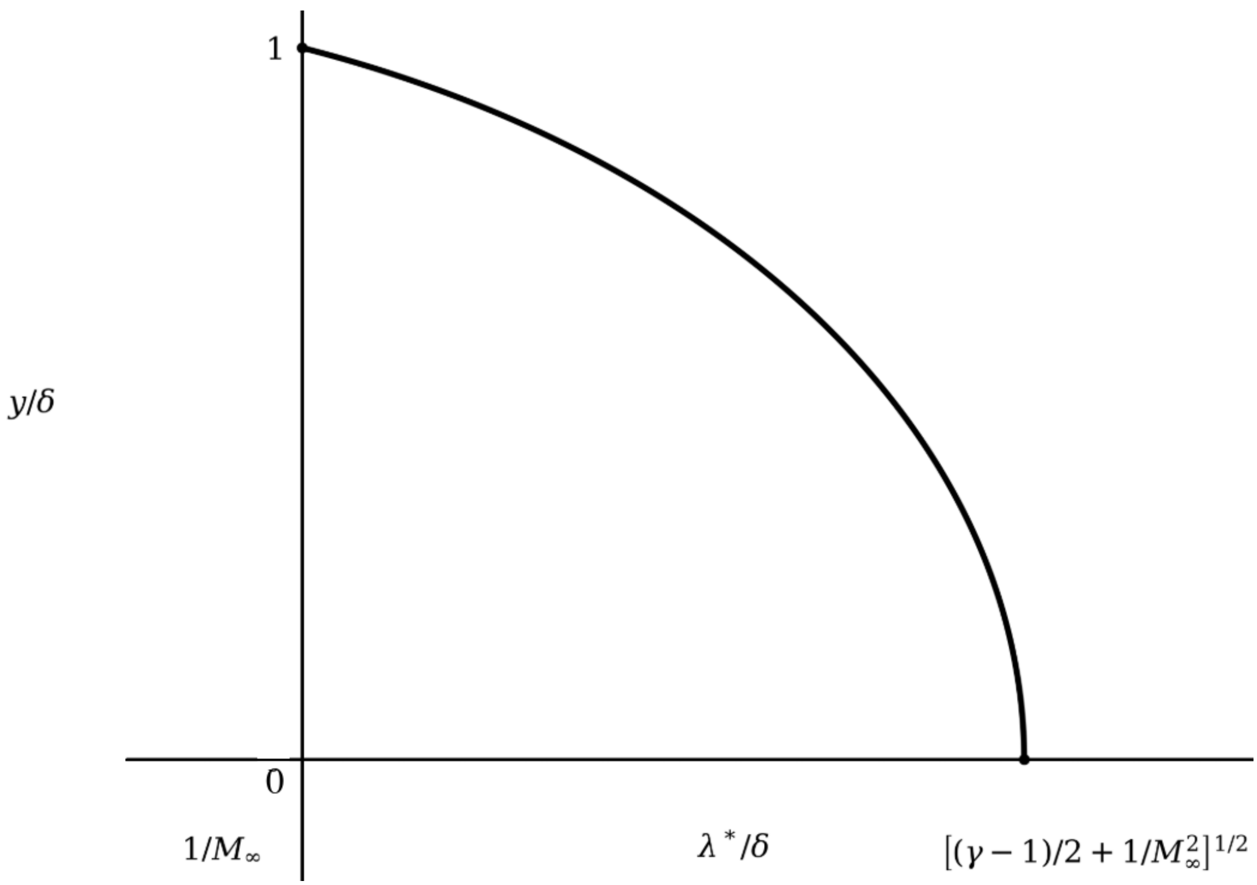

Figure 2.1: Schematic variation of sonic-eddy size across an idealized hypersonic boundary layer. The curve represents the wall-normal dependence of λ^*/δ derived in Section 2.2. The sonic-eddy size decreases from $[(\gamma-1)/2 + 1/M_\infty^2]^{1/2}$ near the wall to $(1/M_\infty)$ at the boundary-layer edge.

The transport implications of this result can be interpreted using Corrsin's criterion, which states that gradient-diffusion or eddy-viscosity models are physically appropriate only when the largest eddies responsible for transport are small compared with the distance over which transport occurs. In the present problem, that distance is the height above the wall, y. The boundary between a diffusion-like region and a non-diffusive region is therefore estimated by setting the sonic-eddy size equal to the wall distance,

$$\lambda^* = y_d \text{ or } \frac{\lambda^*}{\delta} = \frac{y_d}{\delta}$$

Combining this with the preceding result yields

$$\frac{y_d}{\delta} = \left(\frac{2}{\gamma + 1}\right)^{1/2} \frac{a_t}{U_\infty} = \left[\frac{\gamma - 1}{\gamma + 1} + \frac{2}{(\gamma + 1)M_\infty^2}\right]^{1/2}$$

Above y_d, the sonic eddies are small compared with the local transport distance and a diffusion-like interpretation is plausible. Below y_d, the sonic eddies are no longer small compared with the wall distance, so a local gradient-diffusion picture is no longer an appropriate physical description, even though transport is still controlled by sonic eddies.

A central consequence of the model is that both the local sound speed and the sonic-eddy size reach their minimum values at the outer edge of the boundary layer, $y/\delta = 1$. If the effective eddy diffusivity is taken to scale as

$$\varepsilon_t \sim a\,\lambda^*$$

then the minimum of both factors at the outer edge implies that turbulent transport is slowest there. The outer region therefore acts as a bottleneck for momentum transfer from the freestream into the boundary layer. Within this framework, the nearly linear velocity profile is interpreted not as an assumed empirical law alone, but as a consequence of the fact that transport is much less restrictive everywhere inside the layer than it is at the edge. Breidenthal further argues that momentum is transported across the outer edge by sonic eddies with characteristic velocity of order a_∞, which under the model assumptions leads to the inverse-Mach skin-friction scaling

$$C_f \propto \frac{a_\infty}{U_\infty} \propto M_\infty^{-1}$$

In the present thesis, these relations are treated as model predictions to be examined against the numerical results presented in Chapter 3.

2.3 Classical Wall Scaling and Comparison Quantities

To compare the sonic-eddy framework with numerical results, it is necessary to define the wall-scaled and integral quantities used throughout the remainder of this thesis. These quantities provide a standard basis for interpreting the simulation data and for relating the computed boundary-layer behavior to classical descriptions of wall-bounded turbulence.

The wall shear stress is denoted by τ_w and is used to define the friction velocity

$$u_\tau = \sqrt{\frac{\tau_w}{\rho_w}}$$

where ρ_w is the density at the wall. Using this scale, the conventional inner variables are defined as

$$u^+ = \frac{\overline{u}}{u_\tau} \ , \ y^+ = \frac{\rho_w u_\tau y}{\mu_w} = \frac{y u_\tau}{\nu_w}$$

where $\bar{u}$ is the mean streamwise velocity, μ_w is the dynamic viscosity at the wall, and $\nu_w = \mu_w/\rho_w$ is the kinematic viscosity at the wall. These quantities are used when comparing the computed near-wall behavior with classical inner scaling.

The skin-friction coefficient is defined using freestream reference quantities as

$$C_f = \frac{2\tau_w}{\rho_\infty U_\infty^2}$$

where ρ_∞ and U_∞ are the freestream density and velocity, respectively. In the present work, this definition is used directly when comparing wall-shear behavior across Mach number. Because the sonic-eddy model predicts a Mach-dependent trend in the transport-limiting behavior of the boundary layer, C_f serves as one of the principal comparison quantities in the later results.

In addition, the streamwise development of the boundary layer may be referenced using the freestream Reynolds number based on distance from the leading edge,

$$Re_x = \frac{\rho_\infty U_\infty x}{\mu_\infty} = \frac{U_\infty x}{\nu_\infty}$$

where x is the streamwise coordinate measured from the plate leading edge. When convenient, the corresponding unit Reynolds number may also be written as

$$Re' = \frac{\rho_\infty U_\infty}{\mu_\infty}, Re_x = Re' x$$

These quantities are useful for describing the downstream evolution of the boundary layer using freestream reference properties.

The quantities required for these definitions are obtained directly from the computed flow fields generated by the Reynolds-stress-model simulations. In particular, the wall shear stress and mean velocity distributions are used to evaluate the wall-scaled quantities and comparison metrics employed in Chapter 3. These definitions provide a consistent framework for relating the classical wall-scaled description of the boundary layer to the transport-based predictions of the sonic-eddy model.

2.4 Governing Equations and Reynolds-Stress-Model Formulation

The present computations are based on the compressible Reynolds-averaged Navier–Stokes (RANS) equations for a three-dimensional hypersonic boundary layer over a flat plate. Because the flow is compressible, the governing equations are written in Favre-averaged form, in which density-weighted averaging is used for the velocity field. In the present study, air is modeled as an ideal gas, the energy equation is retained, and viscous heating is included so that the thermodynamic and compressibility effects relevant to hypersonic boundary layers are represented.

The Favre-averaged continuity equation is

$$\frac{\partial \bar{\rho}}{\partial t} + \frac{\partial}{\partial x_j}\left(\bar{\rho}\tilde{u}_j\right) = 0$$

where $\bar{\rho}$ is the mean density and $\tilde{u}_j$ is the Favre-averaged velocity component. The corresponding momentum equation is

$$\frac{\partial}{\partial t}(\bar{\rho}\tilde{u}_i) + \frac{\partial}{\partial x_j}\left(\bar{\rho}\tilde{u}_i\tilde{u}_j\right) = -\frac{\partial \bar{p}}{\partial x_i} + \frac{\partial \bar{\tau}_{ij}}{\partial x_j} - \frac{\partial}{\partial x_j}\left(\bar{\rho}R_{ij}\right)$$

$$R_{ij} = \widetilde{u_i''u_j''}$$

where $\bar{p}$ is the mean pressure, $\bar{\tau}_{ij}$ is the mean viscous stress tensor, and $R_{ij} = \widetilde{u_i''u_j''}$ is the Favre-averaged Reynolds-stress component associated with turbulent velocity fluctuations. The turbulent stress contribution enters the mean momentum equation through the term $-\frac{\partial}{\partial x_j}\left(\bar{\rho}R_{ij}\right)$. In contrast to linear eddy-viscosity models, this term is not represented solely through a scalar turbulent viscosity; instead, transport equations are solved for the Reynolds-stress components themselves, while additional closure models are used for pressure-strain redistribution, dissipation, and turbulent diffusion.

The total-energy equation is written as

$$\frac{\partial(\bar{\rho}\tilde{E})}{\partial t}+\frac{\partial\{(\bar{\rho}\tilde{E}+\bar{p})\tilde{u}_j\}}{\partial x_j}=\frac{\partial(\tilde{u}_i\bar{\tau}_{ij}-\bar{q}_j)}{\partial x_j}-\frac{\partial(\bar{\rho}\widetilde{u_j''h''})}{\partial x_j}$$

where $\tilde{E}$ is the Favre-averaged total energy per unit mass, $\bar{q}_j$ is the molecular heat flux, and $\bar{\rho}\,\widetilde{u_j''h''}$ denotes the turbulent heat flux. For a Newtonian fluid, the viscous stress tensor is

$$\bar{\tau}_{ij}=\mu\left(\frac{\partial\tilde{u}_i}{\partial x_j}+\frac{\partial\tilde{u}_j}{\partial x_i}-\frac{2}{3}\delta_{ij}\frac{\partial\tilde{u}_k}{\partial x_k}\right)$$

and the molecular heat flux is modeled by Fourier's law,

$$\bar{q}_j=-k\frac{\partial\tilde{T}}{\partial x_j}$$

where μ is the dynamic viscosity, k is the thermal conductivity, and $\tilde{T}$ is the Favre-averaged temperature. The fluid is treated as an ideal gas, so that

$$\bar{p}=\bar{\rho}R\tilde{T}$$

where R is the specific gas constant. In the present work, the specific heat and thermal conductivity are taken as constants, while the dynamic viscosity is modeled using Sutherland's law,

$$\mu(T)=\mu_{ref}\left(\frac{T}{T_{ref}}\right)^{3/2}\frac{T_{ref}+S}{T+S}$$

where μ_{ref}, T_{ref}, and S are the reference viscosity, reference temperature, and Sutherland constant, respectively.

Closure of the Reynolds stresses is provided by the Reynolds Stress Model (RSM) using the Stress-BSL formulation available in ANSYS Fluent. In this approach, transport equations are solved for the Reynolds stresses, while the Stress-BSL model provides an ω-based scale formulation together with near-wall and outer-region blending appropriate for boundary-layer flows. In compact form, the transport equation for a Reynolds-stress component may be written as

$$\frac{\partial}{\partial t}\left(\bar{\rho}R_{ij}\right) + \frac{\partial}{\partial x_k}\left(\overline{\rho\widetilde{u_k}}R_{ij}\right) = P_{ij} + \Phi_{ij} - \varepsilon_{ij} + D_{ij}$$

where $R_{ij} = \widetilde{u_i''u_j''}$, and P_{ij}, Φ_{ij}, ε_{ij}, and D_{ij} represent production, pressure–strain redistribution, dissipation, and diffusion, respectively. This class of model is particularly attractive for the present work because it provides an anisotropic turbulence closure and therefore offers a more direct representation of the turbulent stress field than linear eddy-viscosity models.

In the present study, the computations were performed in ANSYS Fluent using a steady, density-based implicit formulation. The viscous model was specified as the Reynolds Stress (5-equation) model with the Stress-BSL option, and both compressibility effects and viscous heating were enabled. The resulting formulation provides the mean-flow framework used in this thesis to examine whether the transport trends predicted by the sonic-eddy model are reflected in the computed hypersonic boundary-layer behavior. Details of the computational domain, mesh design, and numerical settings are provided in Sections 2.5 and 2.6.

2.5 Computational Domain and Boundary Conditions

The numerical simulations were performed for a three-dimensional flat-plate configuration intended to represent a canonical hypersonic turbulent boundary layer developing over an adiabatic wall. The computational domain had dimensions

$$L_x = 0.3 \text{ m}, L_y = 0.05 \text{ m}, L_z = 0.05\text{m}$$

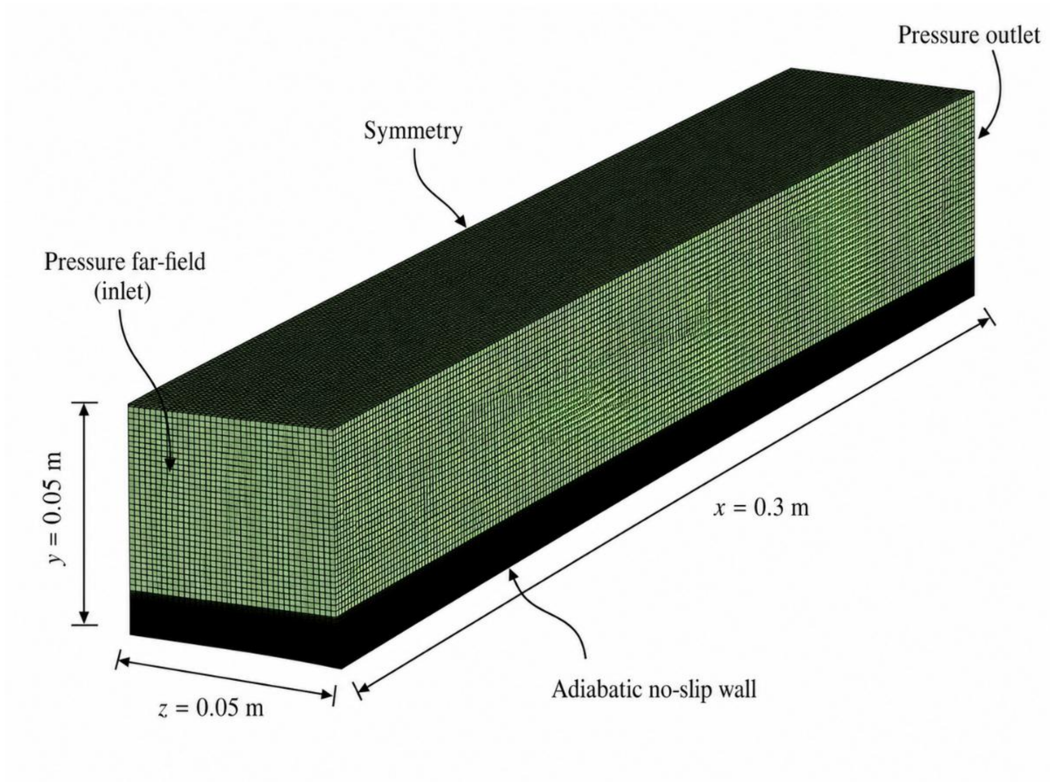

Figure 2.2: Computational domain and boundary conditions used for the hypersonic flat-plate simulations.

where x, y , and z denote the streamwise, wall-normal, and spanwise directions, respectively. The flat plate begins at $x = 0$, and the boundary layer develops in the positive streamwise direction. The computational domain and boundary conditions are shown in Figure 2.2.

A pressure far-field boundary condition was prescribed at the inlet, while a pressure-outlet boundary condition was applied at the downstream boundary. The upper boundary of the domain was treated as a symmetry plane in order to represent the freestream region above the boundary layer. The lower boundary was specified as an adiabatic no-slip wall, consistent with the wall condition used throughout the present study. This configuration was chosen to isolate the development of a nominally canonical hypersonic boundary layer while minimizing additional geometric effects.

The simulations were carried out for a Mach-number sweep spanning $M_\infty = 4.0$ to 7.5, with intermediate cases at increments of 0.5. For the final set of cases considered in the present study, the freestream conditions were selected such that the unit Reynolds number remained fixed,

$$Re' = \frac{\rho_\infty U_\infty}{\mu_\infty} = 1.0 \times 10^7 \text{ m}^{-1}$$

The corresponding freestream and stagnation properties vary with Mach number according to the selected case conditions, and a summary of these values is provided in Table 2.1. This choice allows the influence of Mach number on the boundary-layer behavior and on the transport predictions of the sonic-eddy framework to be examined while limiting variations associated with changes in unit Reynolds number.

Table 2.1: Freestream conditions for the hypersonic flat-plate simulations at fixed ($Re' = 1.0 \times 10^7$ m^{-1}).

M_∞	T_∞ (K)	U_∞ (m/s)	ρ_∞ (kg/m^3)	p_∞ (kPa)	T_0 (K)	p_0 (MPa)
4.0	216.60	1180.14	0.12044	7.4883	909.7	1.137
4.5	217.65	1330.87	0.10723	6.6994	1099.1	1.939
5.0	218.70	1482.30	0.09666	6.0684	1312.2	3.211
5.5	219.75	1634.44	0.08802	5.5521	1549.2	5.166
6.0	220.80	1787.28	0.08081	5.1219	1810.6	8.087
6.5	221.75	1940.39	0.07470	4.7550	2095.5	12.340
7.0	222.70	2094.12	0.06946	4.4406	2405.2	18.380
7.5	223.65	2248.48	0.06492	4.1681	2739.7	26.820

The present domain and boundary-condition setup provide a controlled environment for comparing the computed wall-bounded flow behavior with the theoretical predictions of the sonic-eddy model developed in Sections 2.1 and 2.2. In particular, the flat-plate geometry and adiabatic wall condition allow the effects of Mach number on skin friction and boundary-layer development to be examined in a simplified but physically relevant configuration.

2.6 Grid Design and Numerical Setup

The computational mesh was designed to resolve the near-wall viscous sublayer and to provide sufficient spatial resolution through the boundary-layer region relevant to the present study. Particular attention was given to maintaining a fine wall-normal resolution at the adiabatic wall and to refining the portion of the domain in which the theoretical sonic-eddy length scale was expected to be important. In the present simulations, the first cell height at the wall was set to 3.5×10^{-5} m, corresponding to a wall resolution of approximately $y^{+} \approx 0.5$. This ensured direct resolution of the viscous sublayer in the Reynolds-stress-model calculations.

A structured inflation layer was employed adjacent to the wall. The inflation mesh used a first-layer thickness of 3.5×10^{-5} m , a growth rate of 1.02, and up to 100 inflation layers. Outside the near-wall region, the mesh was generated using a quadrilateral-dominant method with a nominal edge size of 1.0×10^{-3} m. Additional refinement was applied in the boundary-layer region so that the grid remained sufficiently fine relative to the theoretical sonic-eddy length scale. In this way, the mesh design was guided not only by the need to resolve the viscous sublayer, but also by the need to maintain adequate spatial resolution in the part of the flow where the sonic-eddy model predicts transport-relevant structure. The final three-dimensional mesh contained approximately 1.464×10^{6} cells.

The numerical simulations were performed in ANSYS Fluent using a steady, density-based implicit formulation for the compressible flow and energy equations. Spatial discretization employed the Roe-FDS scheme together with a Green–Gauss cell-based gradient evaluation and a third-order MUSCL reconstruction for the mean flow variables. For the turbulence closure, the

Reynolds Stress Model with the Stress-BSL option was used. The specific dissipation rate and Reynolds-stress transport equations were discretized using first-order upwind schemes. Air was modeled as an ideal gas, with constant specific heat and thermal conductivity, while the dynamic viscosity was evaluated using Sutherland's law. Both compressibility effects and viscous heating were enabled.

To promote stable convergence of the Reynolds-stress-model simulations, the under-relaxation factors were adjusted for selected turbulence variables. In the present setup, the under-relaxation factor was set to 0.8 for the specific dissipation rate and 0.5 for the Reynolds stresses, while the turbulent viscosity retained the default value of 1.0. The simulations were monitored using equation residuals, with convergence criteria of 10^{-4} for continuity, momentum, energy, and ω, and 10^{-5} for the Reynolds-stress equations. The final solutions were obtained as steady converged fields and therefore did not require time averaging.

The resulting grid and solver configuration were chosen to provide a consistent numerical framework for examining Mach-number effects in hypersonic boundary-layer development while retaining sufficient near-wall resolution for comparison with the sonic-eddy transport model. In particular, the combination of viscous-sublayer resolution, boundary-layer refinement, and anisotropic turbulence closure was intended to capture the mean flow behavior and wall-shear trends relevant to the theoretical predictions developed earlier in this chapter.

2.7 Post-Processing and Extraction of Skin-Friction Data

The quantities used for analysis in the present study were obtained directly from the converged steady solutions computed in ANSYS Fluent. Because the final simulations were performed as steady Reynolds-stress-model calculations, no time averaging was required. The post-processing procedure was therefore based on the wall-resolved mean flow field obtained after residual convergence had been achieved.

The principal comparison quantity used in this thesis is the skin-friction coefficient, defined in terms of freestream reference quantities as

$$C_f = \frac{2\tau_w}{\rho_\infty U_\infty^2}$$

where $\tau_w$is the local wall shear stress, and ρ_∞ and U_∞ are the freestream density and velocity, respectively. In the present work, C_f was evaluated directly from the wall shear stress reported by ANSYS Fluent. To do this, a post-processing expression based on the wall shear stress was defined within Fluent, and the resulting data were extracted along the wall as a function of streamwise location x.

To describe the downstream development of the boundary layer, the extracted skin-friction data were subsequently expressed in terms of the freestream Reynolds number based on distance from the leading edge,

$$Re_x = \frac{\rho_\infty U_\infty x}{\mu_\infty} = \frac{U_\infty x}{\nu_\infty}$$

where x is the streamwise coordinate measured from the plate leading edge, and μ_∞ and ν_∞ are the freestream dynamic and kinematic viscosities, respectively. Thus, the primary results presented in Chapter 3 are based on the streamwise variation of C_f plotted as a function of Re_x.

After the wall data were extracted from Fluent, the corresponding C_f and Re_x values were processed and plotted using Python. This procedure provided a consistent basis for comparing the simulated skin-friction behavior across the Mach-number sweep and for examining whether the computed trends were consistent with the transport-based predictions of the sonic-eddy model. Although the theoretical sonic-eddy length scale was used earlier as a guiding measure in the mesh design, the comparisons presented in the following chapter are based directly on the computed wall-shear behavior of the final numerical solutions.

2.8 Chapter Summary

This chapter presented the theoretical and numerical framework used in the present study. First, the sonic-eddy model for hypersonic turbulent boundary layers was introduced, and the principal assumptions underlying the model were described. The corresponding scaling relations were then developed, including the wall-normal variation of sonic-eddy size, the definition of the diffusion-limit location, and the transport-based interpretation of the outer region as a bottleneck for momentum transfer. The classical wall-scaled quantities and comparison metrics used throughout the thesis were also defined.

The chapter then described the numerical methodology used to examine these theoretical predictions. The governing compressible Reynolds-averaged equations and the Reynolds-stress-model formulation were presented, followed by the computational domain, boundary conditions, mesh design, and numerical settings employed in ANSYS Fluent. Finally, the post-processing procedure used to extract wall shear and skin-friction data and to express the results in terms of the freestream Reynolds number Re_x was outlined. Together, these elements provide the foundation for the results and discussion presented in Chapter 3.

CHAPTER 3: Results and Discussion

3.1 Overview of Cases and Comparison Approach

This chapter presents the numerical results obtained for the hypersonic flat-plate boundary-layer cases introduced in Chapter 2 and examines them in the context of the sonic-eddy transport model. The simulations span freestream Mach numbers from 4.0 to 7.5 in increments of 0.5, with the unit Reynolds number held fixed across the case matrix. The primary objective of the results chapter is to determine whether the computed wall-shear behavior exhibits trends that are broadly consistent with the transport-based predictions of the sonic-eddy framework.

Because the final study is focused on wall-shear behavior and its dependence on Mach number, the principal quantity used for comparison is the skin-friction coefficient,

$$C_f = \frac{2\tau_w}{\rho_\infty U_\infty^2}$$

reported as a function of the freestream Reynolds number based on distance from the leading edge,

$$Re_x = \frac{\rho_\infty U_\infty x}{\mu_\infty}$$

This choice provides a consistent basis for comparing the downstream development of the boundary layer across all simulated cases using freestream reference quantities.

The results are presented in four stages. First, the normalized mean velocity profiles are examined in order to compare the boundary-layer structure across the Mach-number sweep. Next, the streamwise evolution of C_f is examined for the full Mach-number sweep in order to establish the overall wall-shear behavior of the computed boundary layers. The Mach-number dependence of skin friction is then considered more directly by comparing C_f across cases at selected fixed values of Re_x. Finally, the computed trends are compared with the inverse-Mach dependence implied by the sonic-eddy model in order to assess the extent to which the numerical results support the transport-based interpretation developed in Chapter 2.

Throughout this chapter, the emphasis is placed on trend consistency rather than exact one-to-one agreement with the idealized model. The sonic-eddy framework is based on simplified assumptions regarding boundary-layer structure and transport, whereas the numerical solutions reflect the fuller behavior of the modeled hypersonic flow. The purpose of the comparison is therefore to determine whether the computed skin-friction behavior follows the ordering and Mach-number dependence suggested by the sonic-eddy interpretation, and to identify the extent to which that framework provides a useful physical description of the present results.

Before examining the skin-friction behavior, the computed mean streamwise velocity profiles were first compared across the Mach-number sweep. Figure 3.1 shows the normalized mean velocity (u/U_∞) as a function of the wall-normal coordinate y/δ_{99}, where δ_{99} is defined as the wall-normal location at which $u/U_\infty = 0.99$. The wall-normal coordinate is plotted on a logarithmic scale in order to emphasize the near-wall and intermediate regions of the boundary layer. The profiles provide a useful reference for assessing the development of the computed boundary layers before examining the corresponding wall-shear trends.

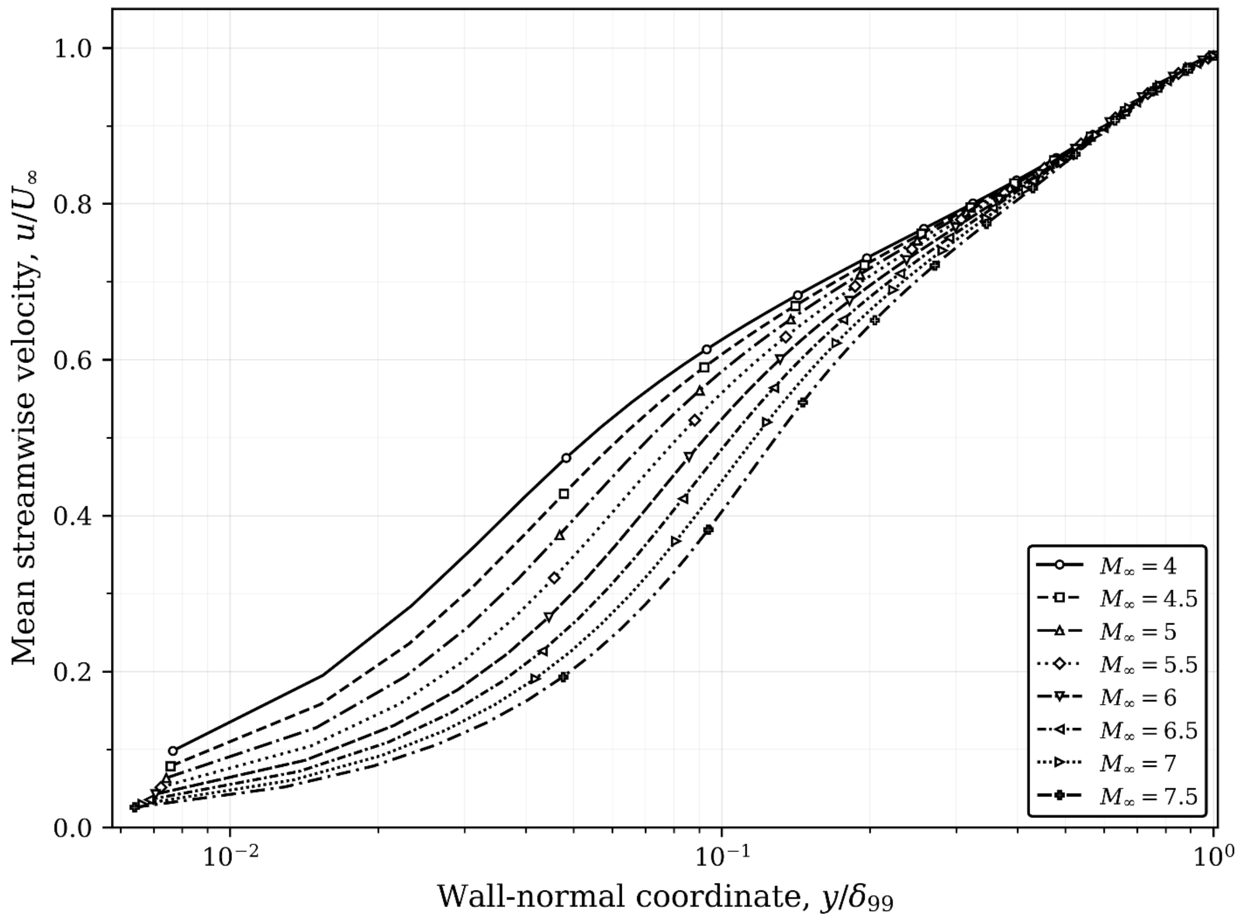

Figure 3.1: Mean streamwise velocity profiles for the Mach-number sweep considered in the present study. The velocity is normalized by the freestream velocity U_∞, and the wall-normal coordinate is normalized by δ_{99}, defined as the location where $u/U_\infty = 0.99$. The logarithmic y/δ_{99} axis emphasizes the near-wall and intermediate boundary-layer regions.

To further illustrate the downstream development of the boundary layer, the mean velocity field was also examined at selected streamwise locations for a representative case. Figure 3.2 provides a schematic representation of the expected development of the streamwise velocity profile over a flat plate. As the boundary layer grows downstream, the region of reduced streamwise velocity extends progressively farther from the wall. This qualitative behavior provides physical context for the skin-friction trends discussed in the following section.

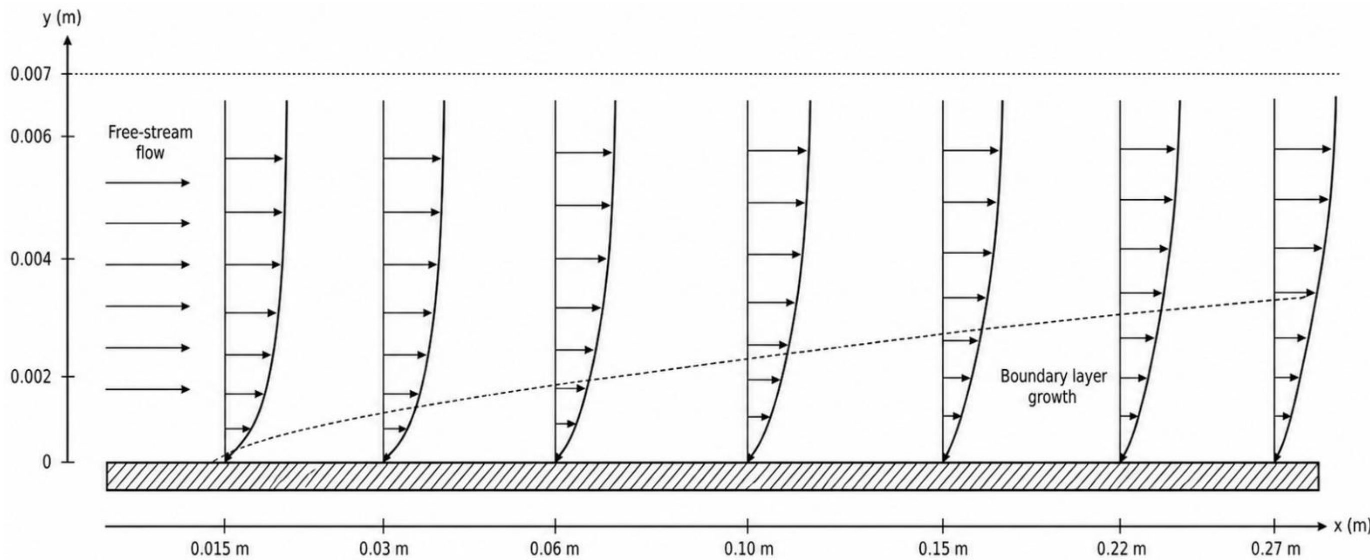

Figure 3.2: Schematic representation of downstream boundary-layer development over a flat plate. The horizontal arrows indicate the local streamwise velocity profile at selected streamwise locations, while the dashed curve illustrates the growth of the boundary-layer thickness with downstream distance.

3.2 Streamwise Development of Skin Friction

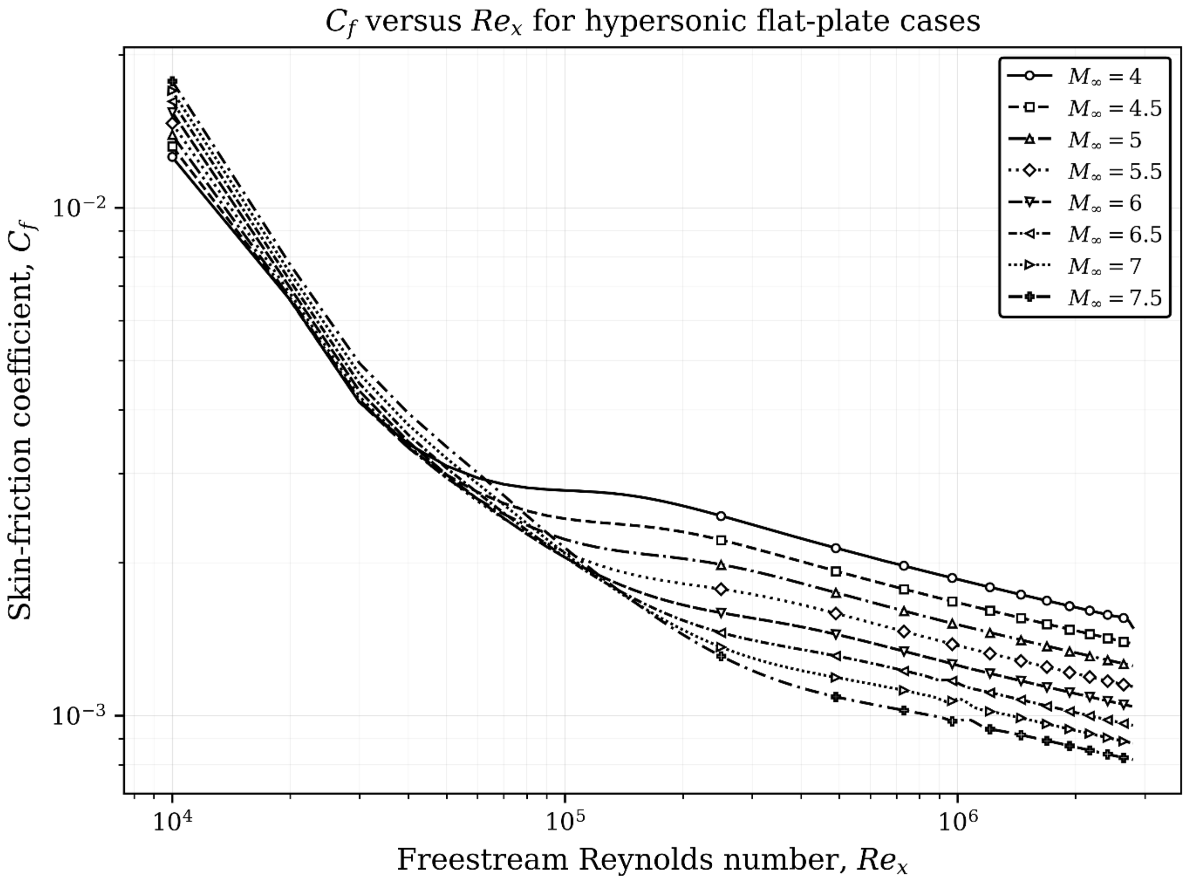

Figure 3.3: Streamwise variation of the skin-friction coefficient C_f with freestream Reynolds number Re_x for the Mach-number sweep considered in the present study.

Figure 3.3 presents the streamwise development of the skin-friction coefficient for the Mach-number sweep considered in the present study, plotted in terms of the freestream Reynolds number Re_x. For all cases, the computed skin-friction coefficient decreases with increasing downstream distance, corresponding to the progressive growth of the boundary layer along the plate. The largest reduction in C_f occurs in the lower-Re_x portion of the domain, after which the curves continue to decrease more gradually downstream.

A comparison across Mach number shows that the cases are relatively close to one another at lower Re_x, but become increasingly separated as the boundary layer develops. Over most of the computational domain, the higher-Mach-number cases exhibit lower values of C_f than the lower-Mach-number cases at comparable Re_x. This ordering becomes clearer in the intermediate and downstream portions of the plate, where the curves are well separated and display a systematic dependence on Mach number. In this sense, the numerical results suggest that the wall-shear behavior is not governed by Reynolds number alone, but is also influenced by the finite-acoustic-signaling constraint associated with increasing freestream Mach number.

3.3 Mach-Number Dependence of Skin-Friction Behavior

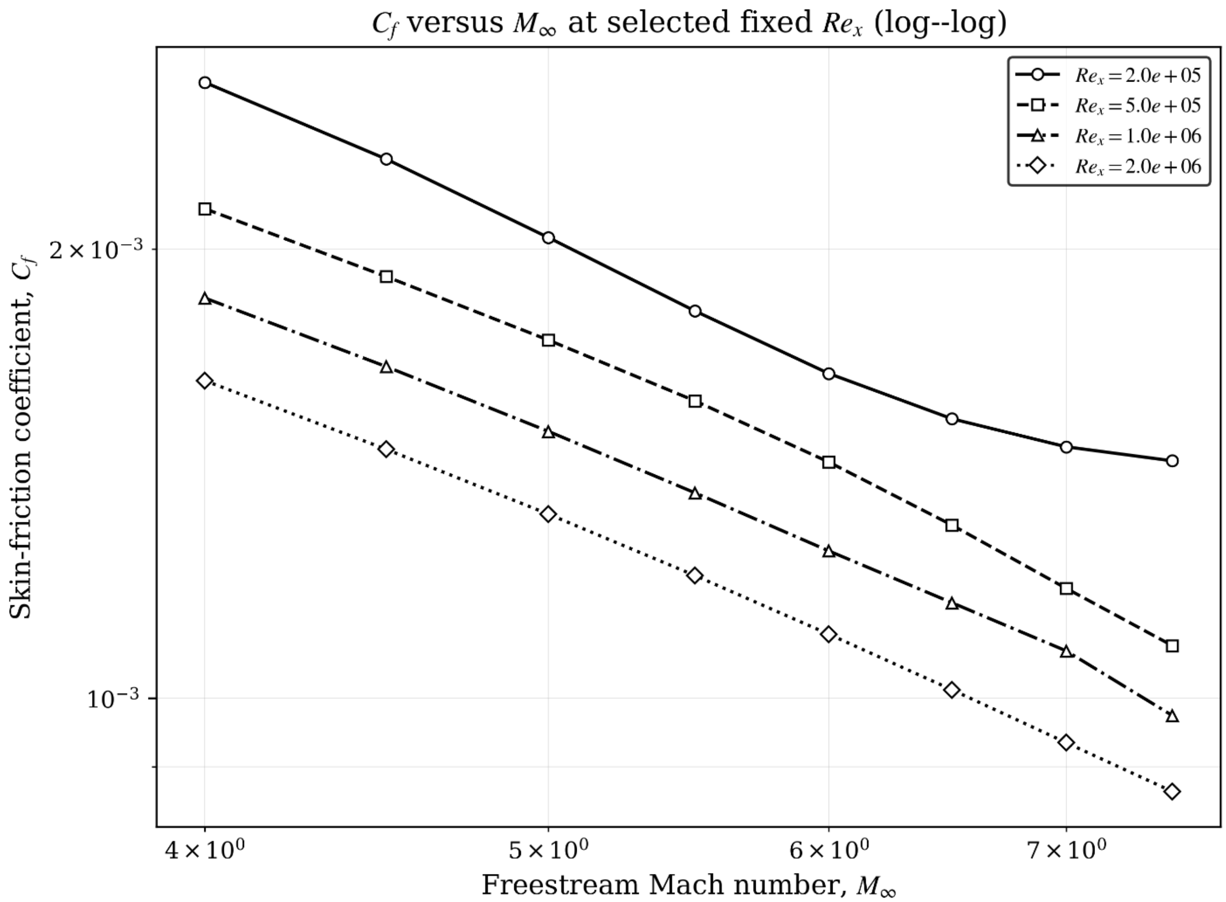

Figure 3.4: Variation of the skin-friction coefficient C_f with freestream Mach number M_∞ at selected fixed values of the freestream Reynolds number Re_x.

To examine the Mach-number dependence of skin friction more directly, the computed values of C_f were compared across the simulated cases at selected fixed values of the freestream Reynolds number Re_x. This approach removes the ambiguity that can arise when interpreting only the full streamwise curves and instead allows the influence of freestream Mach number to be assessed at matched downstream conditions. The selected Re_x values were taken from the common overlap region of all cases so that a consistent comparison could be made across the full Mach-number sweep.

Figure 3.4 shows the variation of C_f with M_∞ at these fixed values of Re_x. For all selected Reynolds numbers, the skin-friction coefficient decreases systematically as the Mach number increases. This trend is consistent with the ordering already observed in Figure 3.3, where the higher-Mach-number cases lie below the lower-Mach-number cases over most of the computational domain. Expressed in this form, however, the Mach-number effect becomes much more explicit: at a given Re_x, increasing the freestream Mach number is associated with a reduction in wall shear.

The reduction of C_f with Mach number is physically significant because it indicates that the wall-shear behavior is not controlled solely by downstream boundary-layer growth. Instead, the trend suggests that finite acoustic signaling speed introduces a systematic constraint on turbulent momentum transport across the Mach-number sweep. In the context of the sonic-eddy model, this behavior is qualitatively consistent with the idea that increasing Mach number strengthens the sonic constraint on the eddies responsible for carrying momentum across the boundary layer.

The results presented in Figure 3.4 therefore provide a more direct comparison of the predicted Mach-number trend of the sonic-eddy interpretation than the streamwise plots alone. Although this comparison does not by itself establish the exact form of the Mach-number scaling, it clearly shows that the computed skin-friction behavior follows the expected ordering with Mach number at matched Re_x.

3.4 Comparison with Sonic-Eddy Scaling

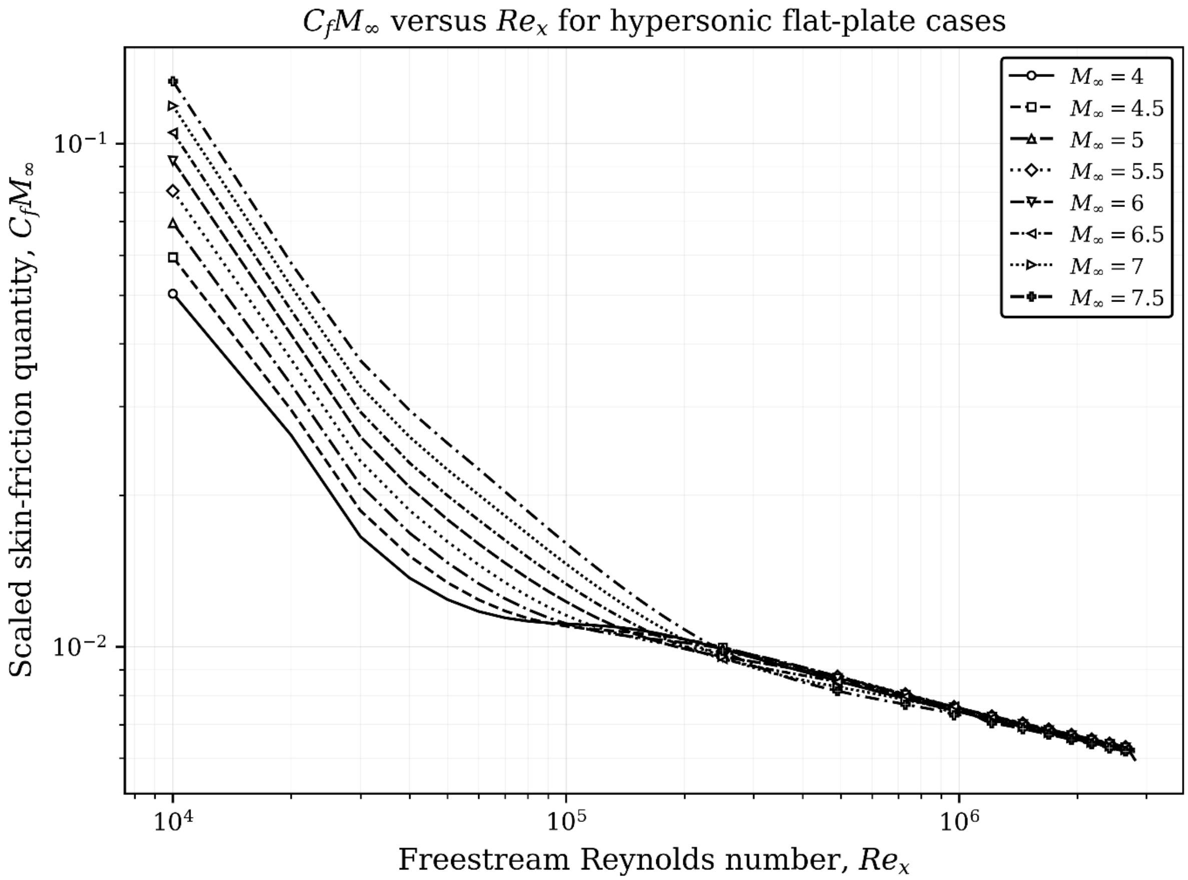

Figure 3.5: Variation of the scaled skin-friction quantity $C_f M_\infty$ with freestream Reynolds number Re_x for the Mach-number sweep considered in the present study.

A more direct comparison with the sonic-eddy model can be made by examining the scaled quantity $C_f M_\infty$ as a function of Re_x. Under the simplified transport argument developed in Chapter 2, the sonic-eddy framework predicts an inverse dependence of skin friction on freestream Mach number, $C_f \propto M_\infty^{-1}$. If this scaling were followed exactly, the quantity $C_f M_\infty$ would collapse to a common curve for all Mach-number cases when plotted against Re_x.

Figure 3.5 shows that such a collapse is not exact over the full computational domain, but a clear degree of collapse is nevertheless observed. In the lower-Re_x portion of the domain, the scaled curves remain noticeably separated, indicating that the computed wall-shear behavior does not follow the inverse-Mach scaling in a strictly exact sense there. As the boundary layer develops downstream, however, the scaled curves move progressively closer together, and over much of the intermediate and downstream region they exhibit a substantially improved collapse compared with the unscaled C_f distributions.

This behavior suggests that the sonic-eddy model captures the principal Mach-number ordering of the skin-friction response, even if the idealized scaling is not recovered perfectly at all streamwise locations. In particular, the improved downstream collapse of $C_f M_\infty$ is consistent with the view that the transport-limiting influence of finite acoustic signaling becomes more clearly expressed once the boundary layer is more fully developed. At the same time, the remaining spread among the curves indicates that the computed flow retains additional Reynolds-number, development, or model-form effects not fully captured by the idealized sonic-eddy argument.

The comparison in Figure 3.5 therefore supports the sonic-eddy framework in a qualitative and trend-based sense rather than as an exact quantitative law over the entire domain. The inverse-Mach scaling implied by the model provides a useful organizing principle for the numerical results, especially in the downstream portion of the plate, where the normalized curves approach one another most closely. This is consistent with the broader conclusion of the present study: the sonic-eddy model offers a physically meaningful interpretation of the Mach-number dependence of skin friction, while still retaining limitations associated with its simplified assumptions and with the numerical modeling framework used here.

3.5 Physical Interpretation and Model Limitations

The results presented in Sections 3.2–3.4 indicate that the computed skin-friction behavior follows a systematic Mach-number dependence over the range of cases considered in the present study. In particular, the skin-friction coefficient decreases with increasing freestream Mach number at matched values of Re_x, and the scaled quantity $C_f M_\infty$ exhibits a substantially improved downstream collapse relative to the unscaled data. Taken together, these trends suggest that the wall-shear response is influenced by the finite-acoustic-signaling constraint emphasized in the sonic-eddy transport model.

From the standpoint of the sonic-eddy framework, this behavior may be interpreted as evidence that increasing Mach number reduces the effectiveness of turbulent momentum transport across the boundary layer. The central idea of the model is that the finite speed of acoustic signaling imposes a constraint on the largest eddies that can remain dynamically coherent, and that this constraint becomes increasingly important as the freestream Mach number rises. Within that interpretation, reduced transport effectiveness in the outer portion of the boundary layer leads naturally to a reduction in the rate at which momentum is supplied toward the wall, and therefore to a reduction in skin friction. The monotonic decrease of C_f with M_∞ observed in the present computations is consistent with this physical picture.

Overall, the results suggest that the sonic-eddy framework captures an important aspect of the Mach-number dependence of wall-bounded momentum transport. While the model is not expected to provide an exact quantitative description of the full computed flow, it offers a useful physical interpretation of the observed skin-friction trends and highlights the possible role of transport limitation in the outer boundary-layer region.

3.6 Chapter Summary

This chapter presented the numerical results for the hypersonic flat-plate boundary-layer cases and examined them in the context of the sonic-eddy transport model. First, the streamwise development of the skin-friction coefficient was presented in terms of the freestream Reynolds number Re_x, showing that C_f decreases downstream for all Mach-number cases and that the curves become increasingly separated with Mach number over much of the domain. The numerical results also showed that, at matched values of Re_x, the skin-friction coefficient decreases systematically with increasing freestream Mach number.

A more direct comparison with the sonic-eddy framework was then made by considering the scaled quantity $C_f M_\infty$. Although the normalized curves did not collapse exactly over the upstream lower-Re_x region, they exhibited substantially improved collapse in the more developed downstream portion of the boundary layer, indicating that the inverse-Mach trend implied by the sonic-eddy model captures an important aspect of the computed wall-shear behavior. The results therefore support the sonic-eddy interpretation in a qualitative and trend-based sense.

CHAPTER 4: Conclusion

The present thesis examined the sonic-eddy transport model as a physics-based interpretation of momentum transfer in hypersonic turbulent boundary layers. The main objective was to assess whether the wall-shear trends predicted by the sonic-eddy framework are reflected in computed hypersonic flat-plate boundary-layer behavior. To this end, three-dimensional Reynolds-stress-model simulations were performed over a Mach-number sweep, with the unit Reynolds number held fixed across the cases.

The theoretical framework was based on the idea that turbulent momentum transport is limited by the largest eddies that can remain dynamically coherent under the requirement of acoustic communication across the eddy. Under the simplified assumptions of the sonic-eddy model, this leads to a transport-limited interpretation in which the outer portion of the hypersonic boundary layer can act as a bottleneck for momentum transfer. As a result, the skin-friction coefficient is expected to decrease with increasing freestream Mach number.

The computed results show a clear downstream decrease of C_f for all cases and a systematic reduction of C_f with increasing M_∞ at matched values of Re_x. When the data are scaled using the quantity $C_f M_\infty$, the curves exhibit a substantially improved collapse in the intermediate and downstream regions compared with the unscaled skin-friction data. Although the collapse is not exact in the upstream lower-Re_x region, the trend is broadly consistent with the inverse-Mach behavior implied by the sonic-eddy framework.

These results support the sonic-eddy model in a qualitative, trend-based sense. The model provides a useful physical interpretation of the reduction of skin friction with increasing Mach number and offers a transport-based perspective on hypersonic wall-bounded momentum transfer. At the same time, the present assessment remains indirect because the Reynolds-stress-model computations do not resolve the eddy-level acoustic communication process itself. Therefore, the agreement should be interpreted as support for the wall-shear consequences of the sonic-eddy model, rather than as direct validation of the detailed eddy-scale mechanism.

Overall, the present study indicates that the sonic-eddy framework captures an important aspect of the Mach-number dependence of skin friction in hypersonic boundary layers. While the model is idealized and not expected to reproduce the computed flow in exact quantitative detail, it organizes the observed trends in a physically meaningful way and highlights the role of transport limitation in interpreting high-speed boundary-layer behavior.

BIBLIOGRAPHY

[1] Breidenthal, R. E., "Sonic Eddy—A Model for Compressible Turbulence," *AIAA Journal*, Vol. 30, No. 1, 1992. DOI: 10.2514/3.10888.

[2] Breidenthal, R. E., *A Simple Model of the Hypersonic Boundary Layer*, University of Washington ResearchWorks, manuscript dated March 24, 2022.

[3] Dintilhac, P., and Breidenthal, R., "Sonic Eddy Model of the Turbulent Boundary Layer," *Fluids*, Vol. 7, No. 1, Article 37, 2022. DOI: 10.3390/fluids7010037.

[4] Neeb, D., Saile, D., and Gülhan, A., "Experiments on a Smooth Wall Hypersonic Boundary Layer at Mach 6," *Experiments in Fluids*, Vol. 59, Article 68, 2018. DOI: 10.1007/s00348-018-2518-z.

[5] ANSYS, Inc., *ANSYS Fluent Theory Guide*, Release **2025 R1**, Canonsburg, PA, **2025**.

[6] Van Driest, E. R., "Turbulent Boundary Layer in Compressible Fluids," *Journal of the Aeronautical Sciences*, Vol. 18, No. 3, pp. 145–160, 1951. DOI: 10.2514/8.1895.

[7] So, R. M. C., Gatski, T. B., and Sommer, T. P., "Morkovin Hypothesis and the Modeling of Wall-Bounded Compressible Turbulent Flows," *AIAA Journal*, Vol. 36, No. 9, pp. 1583–1592, 1998. DOI: 10.2514/2.584.

[8] Rubesin, M. W., "A Modified Reynolds Analogy for the Compressible Turbulent Boundary Layer on a Flat Plate," *NACA Technical Note 2917*, 1953.

[9] Corrsin, S., "Limitations of Gradient Transport Models in Random Walks and in Turbulence," *Advances in Geophysics*, Vol. 18A, pp. 25–60.

[10] Zhang, C., Duan, L., and Choudhari, M. M., "Direct Numerical Simulation Database for Supersonic and Hypersonic Turbulent Boundary Layers," *AIAA Journal*, Vol. 56, No. 11, pp. 4297–4311, 2018. DOI: 10.2514/1.J057296.